Three-dimensional phase-field study of grain coarsening and grain shape accommodation in the final stage of liquid-phase sintering

Hamed Ravash [a], Liesbeth Vanherpe [b], Jef Vleugels [a], Nele Moelans [a,*]

[a] *KU Leuven, Department of Materials Engineering, Kasteelpark Arenberg 44, bus 2450, 3001 Leuven, Belgium*
[b] *Blue Brain Project, EPFL, Chemin des Mines 9, CH-1211 Geneva, Switzerland*

ABSTRACT

A 3-dimensional phase-field model is implemented to simulate the grain evolution in the final stage of liquid-phase sintering. The model considers a liquid phase and a polycrystalline solid phase. Results for varying ratios of the solid–solid interface energy to solid–liquid interface energy and varying solid volume fractions are presented. A variety of microstructures, from fully connected grain structures with liquid pockets at the grain junctions to individual grains fully wetted by the liquid matrix, is seen. The 3 main mechanisms for particle shape accommodation, namely, contact flattening, Ostwald ripening and particle bonding, are reproduced in the simulations. The solid volume fraction, particle size distribution, contiguity, connectivity, particle–particle contact areas and the number of particle contacts per particle are measured as a function of time. The exponent in the power growth law varies between 2.4, for the fully connected grain structures, and 3, for the completely wetted grains.

© 2017 Elsevier Ltd. All rights reserved.

1. Introduction

For materials which are difficult to sinter with the classical approach, liquid phase sintering (LPS), also called liquid phase assisted sintering, is commonly used. In liquid phase sintering, additives are added to the powder to form a liquid phase at temperatures considerably lower than the melting point of the matrix phase. The method is now also widely employed for fabrication of 3D parts in the powder based additive manufacturing [1]. In the final stage of liquid-phase sintering, microstructural evolution of the system is controlled by Ostwald ripening and grain growth.

For a virtually zero particle fraction, the coarsening rate of the particles has been predicted using the analytical models of Greenwood [4], Lifshitz and Slyozov [5], and Wagner [6] in the so-called LSW theory. Later, Ardell [7] and Tsumuraya [8] developed a LSW theory for finite solid volume fractions and others [9–12] incorporated assumptions on the grain shape and the diffusion field around the particles. Very recently, coarsening in systems with high and ultra-high volume fractions (up to 0.96) have been studied using experimental and three-dimensional simulation methods [13–18].

While there exist extensive 3-D simulation studies of microstructure evolution during solid-state sintering [19–23], the studies for liquid-phase sintering are still limited [24–26]. In general, a particle volume fraction larger than 60 vol.% is required for an appropriate geometrical control in liquid phase sintering [2,3], which signifies the importance of a further study of the coarsening processes in solid–liquid systems with high solid volume fractions.

The volume fraction of the solid phase, together with the relative grain boundary and solid–liquid interface energies have a clear effect on the grain shapes and connectivity of the grain structure [3]. For example, in isotropic systems with particle volume fraction $f_p < 70$ vol.%, the grains have an almost spherical shape, except at their contacts with other particles [3]. For higher fractions of the solid phase, the grain faces flatten to eliminate pores and the liquid forms pockets at the grain boundary junctions. The shape of the liquid pockets is determined by the ratio of the grain boundary energy of the solid phase, σ_{ss}, and the solid–liquid interface energy, σ_{sl}. Furthermore, the contacts between two particles grow until they have reached an equilibrium size, called the stable grain–grain contact size, which depends on the particle sizes and the ratio of the solid–liquid and solid–solid interface energies [3].

The mean apparent dihedral angle ϕ at a particle–particle contact [3,27–29] is defined as illustrated in Fig. 1 and given by $2\sigma_{sl}\cos(\phi/2)(1 - s/r) = \sigma_{ss}$, with r the neck radius and s neck surface
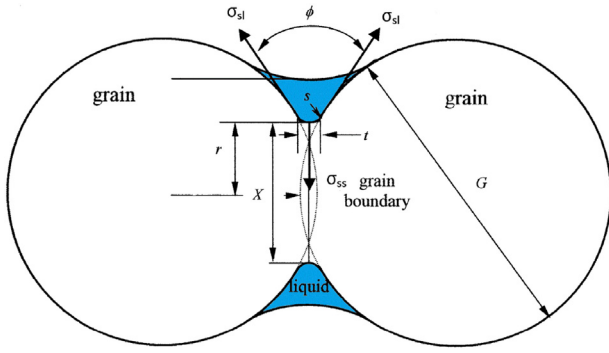
Fig. 1. Schematic illustration of the neck and apparent dihedral angle ϕ formed at the contact between two solid particles in a surrounding liquid phase. r, s, t and X are the neck radius, neck surface radius of curvature, neck thickness and contact size, respectively [3].

radius of curvature. During the neck growth at particle–particle contacts, the apparent or measured dihedral angle may be different from the theoretically expected dihedral angle ϕ^*, as obtained from Young's law $\cos(\phi^*/2) = 0.5\sigma_{ss}/\sigma_{sl}$. The apparent and equilibrium dihedral angles relate as $\cos(\phi/2) = \cos(\phi^*/2) + t/X$, with t the neck thickness and $X = 2r$. In general, a low mean apparent dihedral angle promotes wetting of the grains and facilitates densification. Correlations have been found between the mean apparent dihedral angle and contiguity and connectivity [31,32]. The contiguity C_{ss} is defined as the fraction of solid–solid interface contact area in the microstructure with respect to the total amount of solid–solid and solid–liquid interface area [30]. The connectivity is defined as the average number of particle–particle connections per particle as observed on a random 2D section.

In the presented work, we have performed 3-dimensional simulations based on an adapted phase-field model considering particle volume fractions ranging between $f_p = 0.65$ and $f_p = 0.83$, and solid–solid to solid–liquid interface energy ratios σ_{ss}/σ_{sl} ranging between 1 and 2.5. The important microstructural characteristics were determined as a function of time and particle volume fraction and solid–solid to liquid–solid interface energy ratio. The simulation results are compared with existing empirical laws and different sets of experimental data.

2. Model description

A novel phase-field model is presented, specifically designed to model the liquid phase assisted grain coarsening and grain shape accommodation phenomena in the final stage of LPS. Essentially, the model is an assembly of the interfacial energy description of Moelans et al. [33,34] with a bulk energy description based on the formulation of Folch and Plapp [35].

The interfacial energy description of Moelans et al. allows for an accurate description of interfacial and grain boundary energies in polycrystalline multi-phase structures with inhomogeneous interface properties and avoids the presence of so-called 'third' or 'ghost' phases [36,37] at grain boundaries or interfaces affecting their properties and kinetics.

A great advantage of the bulk energy formulation of Folch and Plapp is that it does not affect the interface properties in the model. It also avoids the presence of solute segregation at grain boundaries of which the magnitude is difficult to control in phase-field models when the diffuse interface width is taken larger than the physical interface width, which is often required because of computational limitations. The onrealistically large solute segregation could affect the kinetics of interface and grain boundary movement [38,39]. The bulk energy formulation of Folch and Plapp assumes a parabolic composition dependence. Although, strictly speaking, a parabolic

composition dependence is thermodynamically inconsistent in the dilute limits $c_i \rightarrow 0$ and $c_i \rightarrow 1$ and generally does not describe the composition dependence well over a large composition range, it is reasonable to apply this simplification when considering coarsening phenomena in bulk materials, since in these processes the compositions of the phases remain close to the equilibrium compositions.

As in the models of [12,33,40], the presented model uses a large set of non-conserved phase-field variables, $\eta_1(\mathbf{r}, t), \ldots, \eta_{p_s}(\mathbf{r}, t)$, which are a function of space $\mathbf{r}$ and time t, representing the different grain orientations in the solid phase. p_s is taken equal to the number of solid phase particles considered in the simulations. An extra non-conserved phase-field variable, denoted as $\eta_{p_s+1}(\mathbf{r}, t)$, is introduced to represent the liquid matrix phase. The non-conserved phase-field variables are defined such that in each grain, one of the η_i (with $i = 1, \ldots, p_s$) equals 1, namely that representing the considered grain, while all the other phase-field variables equal 0. Similarly, within the liquid phase, $\eta_{p_s} + 1 = 1$ and $\eta_{i \neq p_s} + 1 = 0$. At grain boundaries and solid–liquid interfaces, the phase-field variables change their values smoothly. The region where this happens is called the diffuse interface region. Its width is typically chosen based on computational considerations. These phase-field variables are not interpreted as phase fractions and their sum can deviate from 1 over the diffuse interface regions. They are merely used to indicate which phase(s) is(are) present at each point.

The composition variations in the system are described using one conserved phase-field variable $c(\mathbf{r}, t)$, representing the local molar fraction of one of the 2 components (further referred to as the independent component; the other component is called the dependent component) as a function of space and time.

The thermodynamic free energy of the system is modeled to consist of bulk (F_{chem}) and interface (F_{inter}) contributions, namely

$$F = F_{chem} + F_{inter}. \tag{1}$$

Pressure P, temperature T and molar volume V_m are constant throughout the system and in time.

The chemical bulk energy of the system is formulated following the approach of Folch and Plapp [35], giving

$$F_{chem} = \int_V [f_{chem}(\eta_1, \ldots, \eta_{p_s+1}, c)]dV \tag{2}$$

where the integral is taken over the simulation domain with volume V and with f_{chem} as a function of the phase fields $\eta_{1,\ldots,p_s+1}(\mathbf{r}, t)$ and concentration field $c(\mathbf{r}, t)$,

$$
\begin{aligned}
f_{chem}&(\eta_1, \ldots, \eta_{p_s+1}, c) \\
&= \frac{A}{2}\left(c - \left(c_s^0 H_s(\eta_1, \ldots, \eta_{p_s+1}) + c_l^0 H_l(\eta_1, \ldots, \eta_{p_s+1})\right)\right)^2 \\
&\quad + \left(G_s H_s(\eta_1, \ldots, \eta_{p_s+1}) + G_l H_l(\eta_1, \ldots, \eta_{p_s+1})\right),
\end{aligned} \tag{3}
$$

where c_s^0, c_l^0, G_s, G_l and A are model parameters chosen to reproduce the equilibrium compositions of the solid and liquid phase. $H_{s,l}(\eta_1, \ldots, \eta_{p_s+1})$ are functions that interpolate between the composition dependent energy descriptions of the solid and the liquid. As specified by Folch and Plapp, these functions should be chosen such that they obey the following requirements: $H_l = 1$ in the liquid phase (i.e. $\eta_{p_s+1} = 1$, $\eta_{i \neq p_s+1} = 0$), $H_l = 0$ in the solid phase and $\partial H_l/\partial \eta_i = 0$, $i = 1 \ldots p_s + 1$ in both the solid and liquid phase (i.e. where one of the η_i equals 1 and the other 0) and, similarly, $H_s = 1$ in the solid phase, $H_s = 0$ in the liquid phase and $\partial H_s/\partial \eta_i = 0$, $i = 1 \ldots p_s + 1$ in both the solid and the liquid. As the interpolation functions proposed by Folch and Plapp do not extend easily to